Polyethylenimine modified tiger nut residue for removal of Congo red from solution

Alexander Nti Kani, Evans Dovi, Aaron Albert Aryee, Farid Mzee Mpatani, Runping Han*, Zhaohui Li*, Lingbo Qu*

College of Chemistry, Zhengzhou University, No. 100 of Kexue Road, Zhengzhou 450001, China, Tel. +86 371 67781757; emails: rphan67@zzu.edu.cn (R. Han), zhaohui.li@zzu.edu.cn (Z. Li), qulingbo@zzu.edu.cn (L. Qu), mykani@yahoo.com (A. Nti Kani), evansdovy@gmail.com (E. Dovi), a.niiayi@yahoo.com (A.A. Aryee), papilampatani@gmail.com (F.M. Mpatani)

ABSTRACT

A surface-modified tiger nut residue (TNR) was achieved by polyethylenimine (PEI) using glutaraldehyde as a cross-linker at room temperature to enhance the adsorption capacity toward anionic dyes. Surface characterizations confirmed the successful loading of PEI onto the surface of TNR. Preliminary batch experiments were performed to explore the adsorption property of PEI-modified TNR (TNR@PEI) toward Congo red (CR, anionic dye) from the solution. The adsorption was favored at solution pH 5 and at 30°C. The kinetic and isotherm curves were described best by the pseudo-second-order kinetic model and Redlich–Peterson model, respectively. The maximum adsorption capacity of the adsorbent towards CR, as revealed by the Langmuir model, was 197, 274, and 240 mg/g at 20°C, 30°C, and 40°C, respectively. The process was endothermic and spontaneous with a signal of entropy decrease, which followed physical adsorption coupled with electrostatic interaction between the surface of the adsorbent (charged $-NH_3^+$) and the negatively charged moieties of the anionic CR ($-SO_3^-$) under acidic conditions. Besides, TNR@PEI had a good desorption and regeneration performance, hence enhancing its potential to be used as an effective adsorbent to remove the anionic dye.

Keywords: PEI-modified tiger nut residue; Adsorption; Congo red; Regeneration

1. Introduction

Recently environmental pollution, particularly from industrial effluents, is one of the most serious concerns of pollution control experts, as the world witnesses continuous population growth and economic development. The uncontrolled discharge of domestic and industrial wastewaters into the environment is dramatically contaminating water resources. Human health is under threat when these pollutants found their way into water bodies at levels above their allowable limit as set by the various Environmental Agencies and World Health Organization (WHO) [1–3].

The constituents of these effluents may include dyes, pesticides, heavy metals, and polycyclic aromatic hydrocarbons. Synthetic dyes such as Congo red (CR) are an important class of recalcitrant organic compounds that are often found in the environmental media as a result of their extensive application in textiles, paper and leather industries [4–7]. Large quantities of these dyes are annually discharged into the environment as wastewater, which is aesthetically displeasing and undesirable [8].

The attention of environmental scientists' has been drawn to these dye pollutants, and there is engagement in exploring methods for their efficient removal.

* Corresponding authors.

Advance oxidation, coagulation–flocculation, electrochemical, adsorption, membrane separation, ozonation, biological processes, and catalytic degradation have been reported for the removal or degradation of dyes from aqueous solution [9–13]. Among these techniques, adsorption is reported as the most suitable, efficient and superior method due to cost, environmental friendliness, and operational simplicity [6,10,14,15].

Graphene oxides [16], activated carbon [17,18], chitosan [19], carbon nanotubes [20,21], nanomaterials [22–25], agricultural wastes [26,27] and among others have been evaluated as adsorbents in the recent past, however, for economic viability, inexpensive adsorbents such as agricultural wastes are preferred [28]. Agricultural waste, such as tiger nut residue (TNR), was used as a low cost and eco-friendly absorbent to remove methylene blue from aqueous solution efficiently [28]. However, it recorded a relatively small adsorption capacity toward cationic pollutants; hence, the need to modify the surface of TNR to improve its adsorption capacity to realize the full potential of TNR as an adsorbent. According to the authors' knowledge, no comprehensive work has been dedicated to evaluating the adsorption behavior of surface-modified tiger nut residue.

Although reports exist on improved adsorption capacities as a result of surface modification of agricultural waste adsorbents, a literature search reviews none of such studies exist on TNR; hence, this paper details such study for the first time. Oliveira et al. [29] observed a higher adsorption capacity towards phenol when they modified mesoporous silica with 3-aminopropyltriethoxysilane. Similarly, Mpatani et al. [27] modified sugarcane bagasse using citrate and applied the modified bagasse in the adsorption of methylene blue from aqueous solution. Also, Kousha et al. [30] reported a two-fold improved adsorption capacity of brown macroalga towards acid orange II after propylamine surface modification. One of the promising pathways which have the potential to increase adsorption capacity is amine modification. Ong et al. [31] and Wang et al. [32] showed that amino has an active coordinated functional group and that it is easily protonated in acidic conditions. This protonation property is essential for the adsorption of anionic pollutants like CR. Polyethylenimine (PEI) is environmentally friendly and water-soluble with series of $-NH_2$ and $-NH$ groups, which are beneficial for the removal of anionic pollutants and heavy metal ions. Hence, PEI modified TNR may efficiently adsorb anionic dye CR. Amine containing compounds like polyethylenimine and ethylenediamine modified biomass can efficiently adsorb dye pollutants, such as Basic blue 3 and Reactive orange 16 [33], Methyl orange [25], Phenol red [33], Congo red [7], cationic metal ions such as chromium [34], nickel [35], copper [36], lead [37], anionic species such as nitrate, nitrite, cyanide, phosphate, and fluoride, as well as anionic metal complexes such as chromate, arsenate/arsenite, vanadate and selenate/selenite [38].

As far as the authors are aware, there is no published analysis of the surface modification of TNR using PEI to improve its adsorption capacity towards cation dyes. Therefore, in this work, we have reported for the first time the cross-linking of PEI onto TNR and investigated its adsorption efficiency towards model anionic dye (Congo red) as a function of pH of the medium, temperature, contact time, concentration of

the adsorbate moieties, and salts. Besides, the morphological properties of the TNR@PEI were evaluated. To be able to brainwave the mechanism underpinning the adsorption process, we also evaluated some relevant kinetic and isotherms models in addition to thermodynamic parameters.

2. Materials and methods

2.1. Materials

Tiger nut residue (TNR) was soured from Kumasi, Ghana. Congo red (≥98%, CR, $C_{32}H_{22}N_6Na_2O_6S_2$), polyethylenimine (≥99%, PEI), glutaraldehyde (≥25%, GA), absolute ethanol (≥99.9%, C_2H_5OH) were purchased from ALADDIN ReagentCo., Ltd., (Shanghai, China). Sodium sulfate (≥99%, Na_2SO_4), sodium chloride (≥99.5%, NaCl), sodium carbonate (≥99.8%, Na_2CO_3), and sodium hydroxide (≥99%, NaOH) were bought from Zhengzhou Chemical Corporation, China. All reagents and solvents were of analytical reagent grade and used without further purification.

2.2. Preparation of TNR@PEI

The adsorbent (TNR@PEI) used in this work was prepared by a simple facile cross-linking method. Briefly, TNR was prepared following our earlier reported method [28]. 2 g of the TNR was weighed into a conical flask, and 100 mL of 30% PEI was dispensed into it and stirred at room temperature for 12 h. Thereafter, 10 mL of 5% GA was added and stirred for another 2 h at room temperature. The resulting material was washed several times and dried in an oven at 60°C to produce TNR@PEI and subsequently used for characterization and adsorption.

2.3. Morphology and characterization

TNR@PEI was analyzed by the Fourier-transform infrared (FTIR) spectrometer (FTIR, Nicolet iS50, America) to determine functional groups. A scanning electron microscopy (SEM, JEOL 6335F-SEM, Japan) was used to observe the surface morphological structure of the material. Basic elemental analysis was carried out using an elemental analyzer (Thermo Scientific FlashSmart, USA). The crystal structure of the absorbents was examined by powder X-ray diffraction (XRD) (PANalytical, Netherlands). X-ray photoelectron spectroscopy (XPS, ESCALAB 250Xi, England) was employed to analyze TNR@PEI composite films. The absorbance and equilibrium concentration of CR was measured on visible spectrophotometry (PERSEE TU-1900, China) at 500 nm (maximum emission wavelength on CR determined from 3 repeated scans of new CR solutions). The pHzpc (pH of zero point charge) of adsorbents was carried out following the method described by Meili et al. [39].

2.4. Adsorption experiment

The PEI modified TNR (TNR@PEI) dye adsorption performance towards CR was compared with that of the pure TNR through a series of batch processes. The effects of contact time (10–360 min), temperature (20°C–40°C), pH (2.0–10) and dye concentration (20–1,000 mg/L), salts

(NaCl, Na_2SO_4, Na_2CO_3) on the adsorption capacity of the TNR@PEI were studied. The amount of dye adsorbed (q, mg/g) and dye removal efficiency (% P) were calculated using Eqs. (1) and (2). All adsorption experiments were performed in triplicate and the averages were subjected to data analysis to get reliable and validated results. The adsorption quantity of CR (q, mg/g) and the removal efficiency (P, %) were calculated by using the following formula.

$$q = \frac{V(C_0 - C)}{m} \tag{1}$$

$$p = \frac{(C_0 - C)}{C_0} \times 100\% \tag{2}$$

where C_0 = initial CR concentration (mg/L), C = CR concentration at any time t or equilibrium (mg/L), V = volume of the CR solution (L), m = weight of adsorbent (g), p = removal efficiency.

2.5. Desorption and regeneration

The spent TNR@PEI was obtained after adsorption of 100 mg/L of CR at a pH of 5 at 30°C for 6 h. Thereafter, its reusability was evaluated using 0.1 mol/L NaOH solution as the desorbing solvent. The spent TNR@PEI@CR was added to 20 mL desorbing solvent and agitated at 30°C for 6 h. This process was repeated four consecutive times, and the regeneration yield was obtained as the ratio of values of q_e before and after regeneration.

3. Results and discussion

3.1. Characterization of PEI modified TNR

The surface morphology and features of the pristine and the surface-modified adsorbent were studied to understand the surface chemistry. The SEM images (Fig. 1) revealed that the pristine TNR was rugged with surface protuberances showing uneven heterogeneous surface with reduced porosity. In contrast, the modified material offers a relatively smooth surface with no apparent pores observed on the surface; however, the initial structure is maintained. The PEI loading on TNR resulted in an understandable drop in pore volume and pore size while the surface area was slightly increased to 1.78 m^2/g (Table 1).

The results of the elemental analysis were N 1.64%, C 48.3%, H 6.10% for pristine TNR, and N 9.94%, C 41.5%, H 4.40% for TNR@PEI. This confirmed the successful loading of PEI on the surface of TNR. Besides, FTIR spectra (Fig. 2) of the raw and PEI modified TNR also corroborate the presence of NH_2 functional groups on the TNR. The broad and strong band ranging from 3,200 to 3,600 cm^{-1} may be due to the overlapping of O–H and N–H stretching, which is consistent with the peaks at 1,115 and 1,161 cm^{-1} assigned to alcoholic C–O and C–N stretching vibration, thus showing the presence of hydroxyl and amine groups [40] on the TNR surface. The peak of TNR@PEI at 3,416 cm^{-1} reduced after CR adsorption and shifts to 3,424 cm^{-1}. The band at 2,924 cm^{-1} attributed to the vibration peaks of –CH_3 groups is maintained in both TNR@PEI and TNR@PEI@ CR. The peak at 1,632 cm^{-1} on TNR@PEI, which is shifted to 1,635 cm^{-1} after CR adsorption, is attributed to the presence of carbonyl (C=O) functional groups. From the FTIR analysis, it is observed that most peaks diminished or shifted

Table 1
Brunauer–Emmett–Teller (BET) analysis of TNR and TNR@PEI

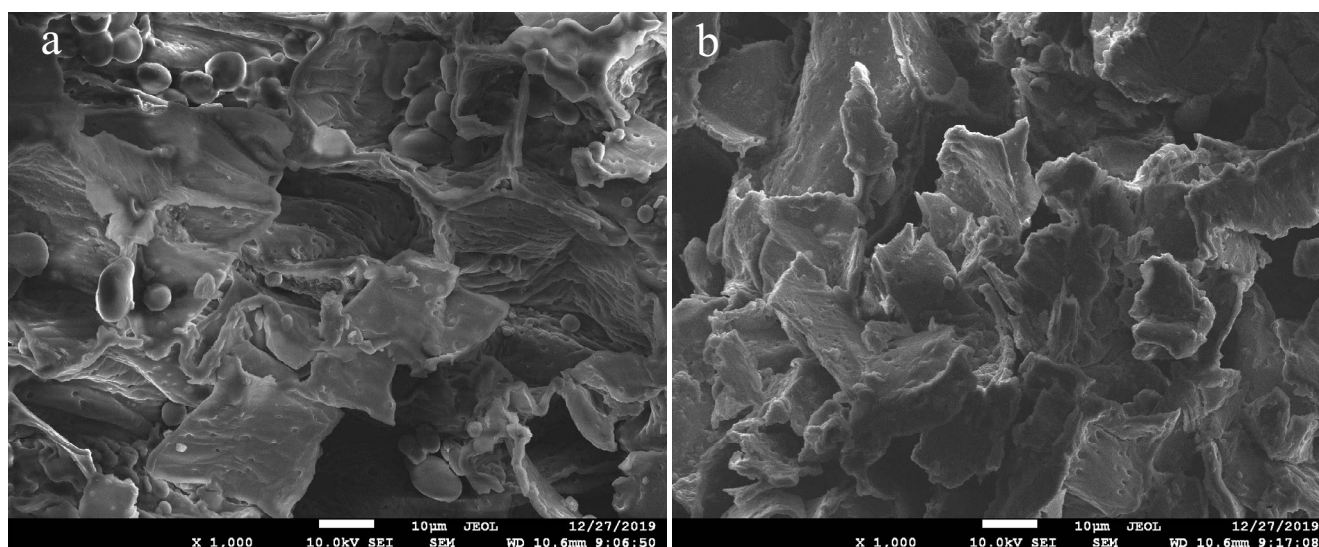| Textural properties	TNR	TNR@PEI
BET surface area (m^2/g)	0.319	1.78
BET total pore volume (cm^3/g)	0.000272	0.000201
BET pore size (nm)	3.42	2.39

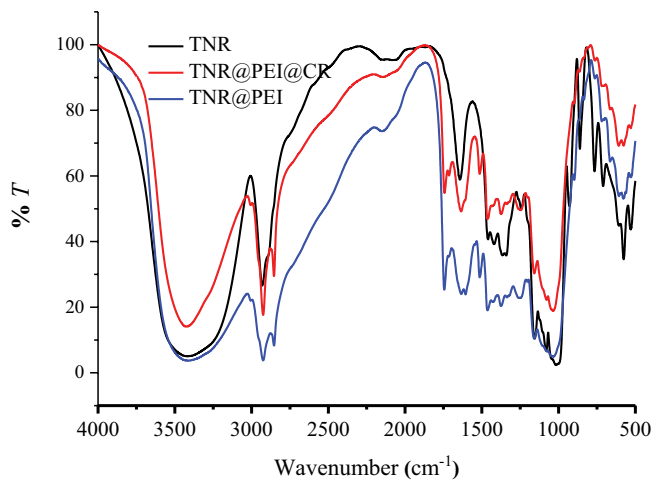Fig. 1. Scanning electron microscopy spectra of (a) TNR@PEI and (b) TNR@PEI@CR.

Fig. 2. Fourier-transform infrared spectra of TNR and TNR@PEI.

Fig. 3. X-ray diffraction patterns of TNR@PEI and TNR@PEI@CR.

slightly after adsorption. This shift in wavenumber and reduced intensity could be due to the adsorbent's interaction with the NH, NH_2, and SO_3^- groups of the CR [18,41].

Fig. 3 shows the XRD diffraction pattern spectra of TNR@PEI and TNR@PEI@CR. Two prominent peaks at 22.50° and 34.90° correspond to planes (200) and (004) indicative of the presence of highly organized crystalline cellulose [28,42]. The result of XRD patterns suggests that the crystalline morphology of TNR@PEI remained unchanged after the adsorption of CR.

The XPS measurements of TNR, PEI modified TNR before and after CR adsorption was performed and presented in Figs. 4a–c, respectively. The increase in the intensity of N1s after PEI modification suggests the increase in the nitrogen content, and the appearance of the S2p can be attributed to the presence of the adsorbed CR on the surface of the TNR@PEI. The high-resolution spectrum XPS pattern of C1s of TNR@PEI before and after the adsorption process (Figs. 4d and e) exhibit the presence of C, H, N, and O, which are attributed to the inherent availability in agricultural waste materials and the existence of element N is attributed to the incorporated PEI molecules. The deconvoluted N1s spectrum of TNR (Fig. 4f) shows peaks at 392.21, 396.78, and 399.59 eV attributed to nitrogen in –NH_2. Whereas, after surface modification by PEI (Fig. 4g), the deconvoluted N1s spectrum of TNR@PEI shows four peaks at 396.40, 398.10, 400.27, and 401.54 eV corresponding to –NH, C–N, N=C, and N–C=O making up 37.3%, 8.1%, 19.0%, and 35.6% respectively. Again, the peaks at 398.10 and 400.27 eV are also attributed to pyridinic nitrogen (=N–), and pyrrolic nitrogen (N–H) from PEI formed during the cross-linking process of PEI onto TNR with glutaraldehyde. Thus, this dataset intensely supports the cross-linking of PEI with the TNR surface during the modification process.

3.2. Adsorption study

3.2.1. Effect of pH on CR Adsorption and the pH of zero point charge (pHzpc) of TNR@PEI

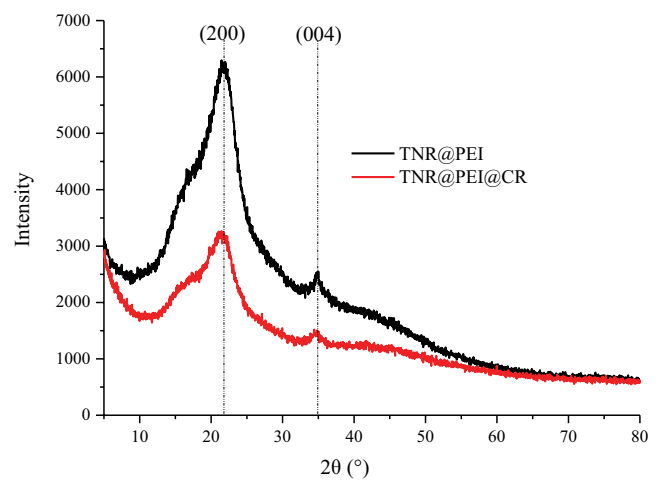The surface charge of the adsorbent is affected by pH through the dissociation of functional groups on the active

sites of the adsorbent as well as the solution dye chemistry [43]. The value of pH at which the surface of TNR@PEI became neutral was found to be 6.0 (Fig. 5a); therefore, at pH below 6, a cationic surface is obtained, which is attractive to CR. This is due to the protonation of the surface of TNR in an acidic medium. The TNR has a reported pHzpc of 5.5 [28]; therefore, it can be suggested that the cross-linking of PEI onto the TNR added some alkaline functional groups on the surface of the material and led to an increase in the isoelectric point. This confirms that PEI had successfully loaded on the TNR to produce the TNR@PEI. It is established that CR is highly sensitive to pH. Since solution pH mediates adsorption, the effect of solution pH on CR adsorption by TNR@PEI was examined from pH 2 to 12, and the results are illustrated in Fig. 5b. It can be observed that CR adsorption increases as the solution pH increases from 2.0 to 5.0 and decreases gradually as the alkalinity of the solution increases up to pH 12. Hence, pH 5 was selected for the adsorption experiments. This observation may be explained by two possible mechanisms. There may be an improved electrostatic interaction between the protonated groups of TNR@PEI and the negatively charged moieties of the anionic CR (–SO_3^-) under acidic conditions. The gradual decrease in the adsorption capacity of CR in the alkaline medium could also be attributed to the competitive adsorption from the excess OH⁻ and the anionic CR as well as the cationic surface of the TNR@PEI in alkaline medium. Some other researchers have reported similar observations [7,44]. However, the q_e of about 60 and 85 mg/g was recorded at highly acidic and alkaline mediums, which suggest some other actions (such as chemical reaction, van der Waals force, or hydrogen bond) might have been present in the adsorption system [7].

3.2.2. Dose effect

To establish the economic viability of an adsorbent, it is imperative to determine the minimum dosage required to remove a dye efficiently [45]. As shown in Fig. 6, the rate of CR removal by TNR@PEI increased with an increase in the adsorbent dosage while the adsorption capacity decreased.
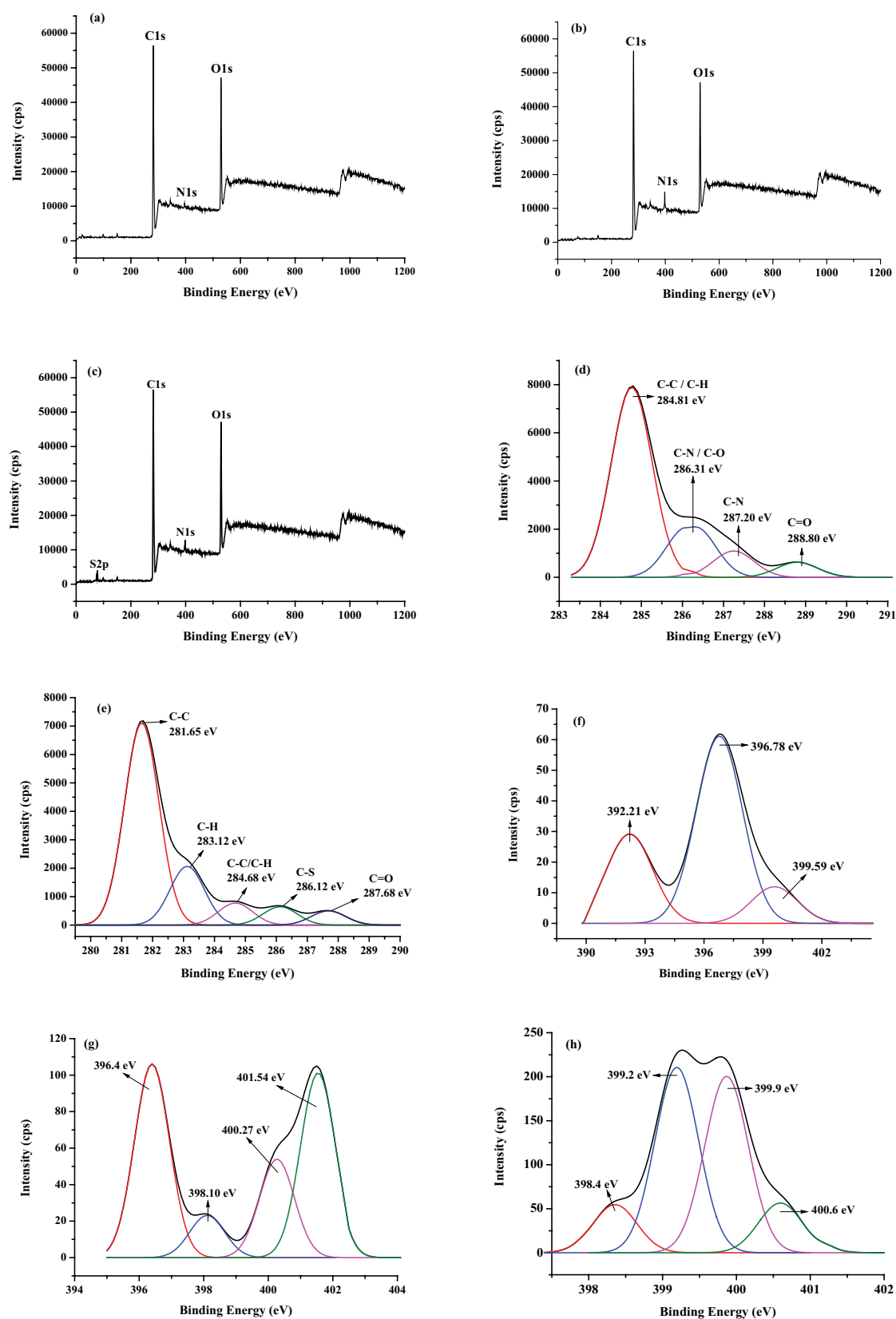
Fig. 4. X-ray photoelectron spectroscopy of (a) TNR, (b) TNR@PEI, and (c) TNR@PEI@CR. High-resolution spectrum of C1s of TNR@PEI (d) before and (e) after the adsorption process. Deconvoluted N1s spectrum of (f) TNR, TNR@PEI, (g) before and (h) after CR adsorption.

Fig. 6. Effect of adsorbent dose on adsorption (T = 30°C; pH = 5; t = 6 h; C_0 = 100 mg/L).
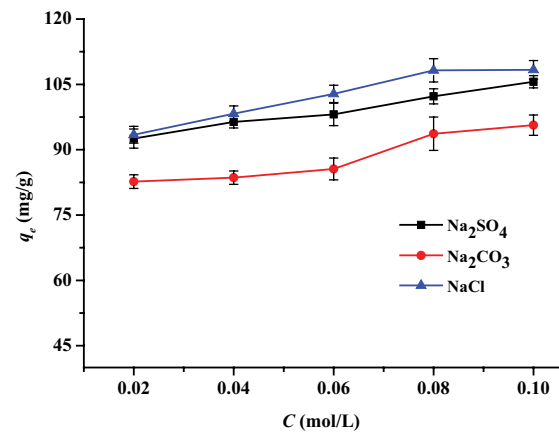
Fig. 7. Effect of salt concentration on CR adsorption by TNR@PEI (T = 30°C; pH = 5; t = 6 h; C_0 = 100 mg/L).
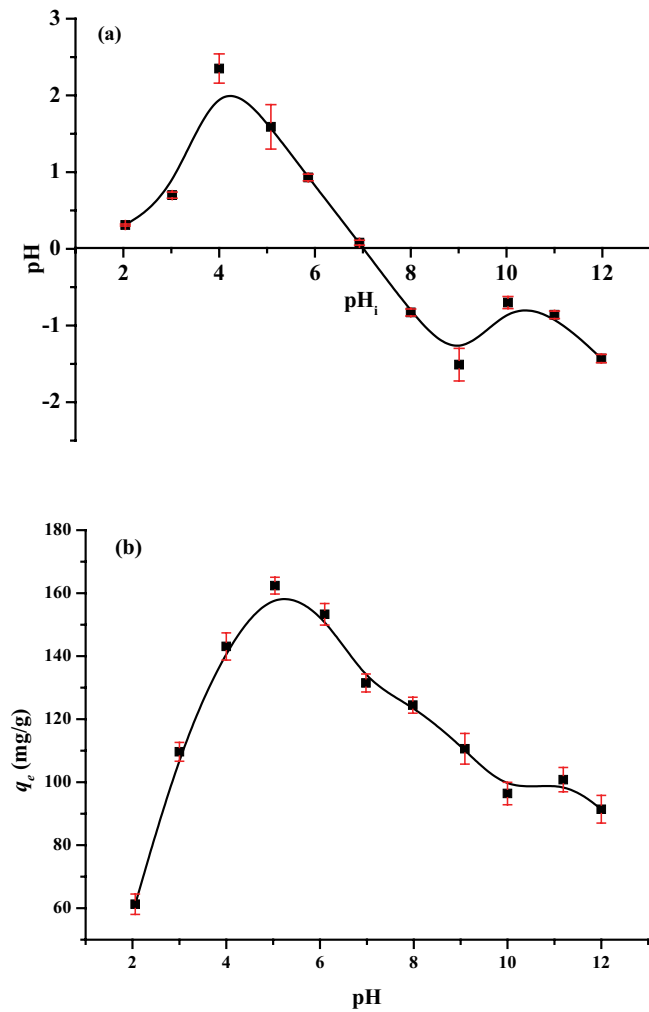
Fig. 5. Measurement of pH of zero point charge (a) and the effect of pH on adsorption (b).

This could be a result of increased adsorption sites available for CR and a large number of active sites remaining unsaturated during the adsorption process, respectively [34].

3.2.3. Effect of salt concentration on CR adsorption

Common salts are mostly presented in wastewater, and their presence may have an effect on adsorption capacity due to their impact on solubility, surface charge, and hydrophobicity of CR. The effect of SO_4^{2-}, CO_3^{2-} and Cl^- on 100 mg/L (pH 5) of CR is presented in Fig. 7. The adsorption capacity of TNR@PEI increased with increasing salt concentration from 0.02 to 0.1 mol/L for all the studies. This could be due to the neutralization effect of the negatively charged surface of the CR in an acidic medium, which makes CR molecules accumulate, precipitate making them easily accessible to the negative actives on the adsorbent, hence increasing the q_e. The lowest q_e was recorded in the presence of Na_2CO_3. This may be due to the slight increase in solution pH when Na_2CO_3 existed in solution. The q_e at high salt concentration also suggests other factors such as hydrogen bond or van der Waals' force

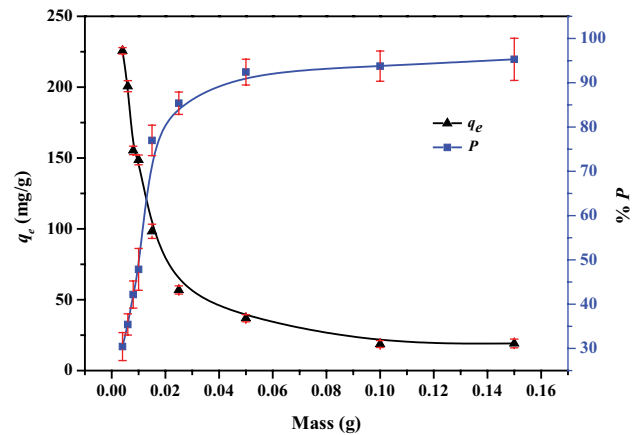may be present in addition to the electrostatic attraction between the adsorbent and the molecules of CR. Similar observations have been reported [8].

3.2.4. Effect of contact time and kinetic modeling

To study the adsorption rate and rate-determining steps in the adsorption process, the effect of contact time was investigated. From Fig. 8, after 90 min, the amount of CR adsorbed did not considerably change with an increase in contact time. Fig. 8 also presents an initial rapid adsorption rate and a subsequent slower process. This two-stage adsorption process may be due to the readily accessible sites on the adsorbent surface, which later reduced after 90 min of contact time, probably due to external mass transfer followed by intra-particle diffusion mass transfer [43]. The experimental data were evaluated with three kinetic models: pseudo-second-order kinetic model (Eq. (3)), intraparticle diffusion equation (Eq. (4)), and Elovich's models (Eq. (5)).

$$q_t = \frac{k_2 q_e^2 t}{1 + k_2 q_e t} \tag{3}$$

$$q_t = k_3 t^{1/2} + C \qquad (4)$$

$$q_t = \frac{\ln(\alpha\beta)}{\beta} + \frac{\ln t}{\beta} \qquad (5)$$

where q_t is adsorption quantity (mg/g) at time t (min), q_e is biosorption capacity at equilibrium (mg/g); k_2 is pseudo-second-order rate constant (mg/g min); A and B are the constants relating to the fraction of the surface covered and chemisorption activation energy; k_3 is constant of diffusion particle and constant C is intercept, which is related to the boundary layer thickness.

It is evident from Table 2 that there were lower values of R^2 and higher values of SSE for intraparticle diffusion and Elovich models; hence, intraparticle diffusion and Elovich models could not properly be used to predict the kinetic process. As there were higher values of R^2 and lower values of sum of squares of the errors (SSE) from pseudo-second-order, it was concluded that pseudo-second-order is better correlative to the experimental data. In addition, the
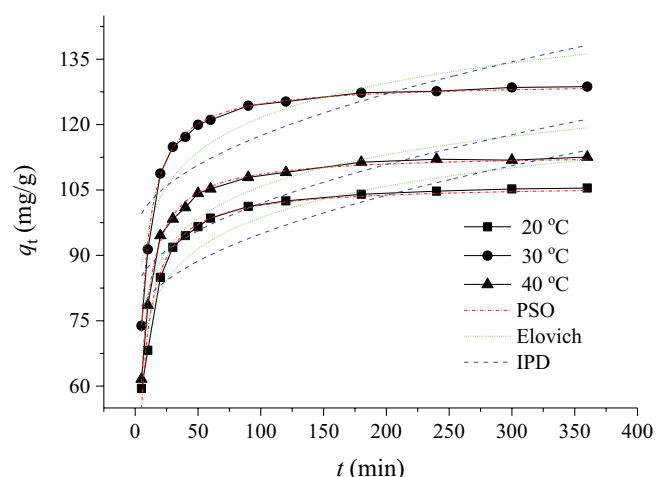
Fig. 8. Contact time and kinetics modeling of CR adsorption onto TNR@PEI (C_0 = 100 mg/L).

experimental adsorption capacities (q_e) of samples were closer to the calculated adsorption capacities of the pseudo-second-order model, and the fitted curves from pseudo-second-order were very close to experimental curves. These suggest again that pseudo-second-order can describe the kinetic process and predict the equilibrium adsorption quantity, while the number of active sites and the initial concentration of the dyes control the adsorption rate, or the whole adsorption process may be controlled by chemisorption [46–48].

3.2.5. Adsorption isotherms curves and modeling

The PEI modified TNR showed enhanced adsorption of CR over the untreated TNR. The adsorption capacity (q_e) of TNR was 113 mg/g whiles that of the surface functionalised, TNR@PEI was 274 mg/g at same condition (pH 5, T = 30°C, t = 6 h, mass = 0.015 g, V = 20 mL). Hence, the surface modification improved the efficiency of adsorption, which may be mainly due to the presence of the series of the amino group, which has a high affinity to bind with the ions of CR in an acidic medium, thus confirming the design concept. The highest adsorptive capacity was recorded at a temperature of 30°C, which implies less energy required. This makes our system more energy-efficient than those reported by Shang et al. [7], Kumar et al. [41], Bayramoglu and Arica [47], in which case the maximum adsorptive capacities were recorded at higher temperatures as 40°C, 50°C and 49.9°C, respectively.

From Fig. 9, the amount of CR adsorbed increased with an increase in equilibrium concentration and ultimately attained a saturated value for all the studied temperatures.

To better understand and validate the adsorption process, Langmuir (Eq. (6)), Freundlich (Eq. (7)), Koble–Corrigan (Eq. (8)), Redlich–Peterson (Eq. (9)), and Temkin (Eq. (10)) isotherm models were applied to the experimental data, and the fitted curves displayed in Fig. 9. The suitability of the model was determined by choosing the model with the value of R^2 closest to 1 and a relatively small SSE.

Langmuir model:

$$q_e = \frac{q_m K_L C_e}{1 + K_L C_e} \qquad (6)$$

Table 2
Kinetic parameters of CR adsorption onto TNR@PEI

Pseudo-second-order	T (°C)	q_e (mg/g)	k_2	R^2	SSE
	20	106 ± 0.802	0.00201 ± 0.000129	0.982	41.8
	30	129 ± 0.313	0.00196 ± 0.000043	0.998	6.71
	40	113 ± 0.319	0.00205 ± 0.0000507	0.997	6.79
Intraparticle diffusion	T (°C)	k_3	C	R^2	SSE
	20	2.14 ± 0.487	73.6 ± 5.2	0.603	932
	30	2.31 ± 0.576	94.3 ± 6.2	0.557	1304
	40	2.15 ± 0.522	80.5 ± 5.6	0.571	1070
Elovich	T (°C)	α	β	R^2	SSE
	20	50.9 ± 5.1	10.4 ± 1.2	0.863	323
	30	69.1 ± 6.4	11.4 ± 1.5	0.828	505
	40	57.2 ± 5.7	10.5 ± 1.3	0.838	404

Note: SSE = $\sum (q - q_c)^2$, q and q_c are adsorption quantity from the experiments and models, respectively.
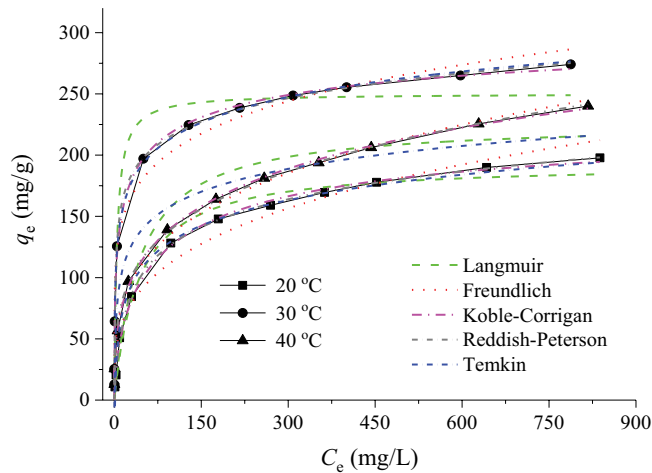
Fig. 9. Adsorption isotherms and fitted curves of CR adsorption onto TNR@PEI.

Freundlich model:

$$q_e = K_F C_e^{1/n} \tag{7}$$

Koble–Corrigan model:

$$q_e = \frac{A_K C_e^n}{1 + B_K C_e^n} \tag{8}$$

Redlich–Peterson model:

$$q_e = \frac{K_{RP} C_e}{1 + a_{RP} C_e^g} \tag{9}$$

Temkin model:

$$q_e = A_T + B_T \ln C_e \tag{10}$$

where q_m represents the monolayer saturation at equilibrium, K_L indicates the Langmuir adsorption isotherm constant related to the adsorption energy. K_F is the Freundlich constant, and $1/n$ (dimensionless) is the Freundlich intensity parameter, which indicates the magnitude of the adsorption driving force or the surface heterogeneity. K_{RP} (L/g) and a_{RP} are the Redlich–Peterson constants, and g (dimensionless) is an exponent whose value must lie between 0 and 1. A, B, and n are the Koble–Corrigan parameters. The values of A_T and B_T are the Temkin isotherm equilibrium binding constant and Temkin constant interaction parameter, respectively.

The obtained isotherm parameters, determined coefficients (R^2), and values of SSE using nonlinear regression are presented in Table 3, while the fitting curves from models are also displayed in Fig. 9. From Table 3, the higher determined coefficients for 20°C (>0.96), 30°C (>0.95), and 40°C (>0.94) from the five models are suggestive that the adsorption of CR by TNR@PEI to be complex and that more than one mechanism mediates the adsorption process. The applicability of these models implies that monolayer

adsorption and heterogeneous surface conditions existed and occurred by multilayer adsorption under the experimental conditions. A comparison of the experimental and fitted curves at 20°C, 30°C, and 40°C (Fig. 9) supports this conclusion. A similar observation has been reported by Zhang et al. [43]. The negative value of one of the Temkin parameters indicates the inadequacy of the isotherm model to explain the adsorption process [17,44,49].

Langmuir adsorption isotherm reviewed maximum monolayer adsorption capacities of 193, 250, and 227 mg/g for temperatures 20°C, 30°C, and 40°C, respectively (Table 3). The values of q_m from this model were lower than those from experimental results. Furthermore, the fitted curves from the Langmuir model were not closer to experimental curves, while the values of SSE were larger. It is implied that the Langmuir model cannot be used to describe the equilibrium adsorption process efficiently.

A fitted Freundlich isotherm with $1/n$ values less than 1 for temperatures 20°C, 30°C, and 40°C represents a good and favorable adsorption process indicting heterogenous multilayer adsorption. Thus, suggesting significant adsorption takes place at low concentrations, but the increase in the amount adsorbed with concentration becomes less significant at higher concentrations and vice versa [43,50,51].

For the Koble–Corrigan model, at high adsorbate concentrations, this model reduces to Freundlich isotherm and that it is only valid when the constant "n" is greater than or equal to 1. Hence, with n values being less than 1 (Table 3) implies that the model is incapable of defining the experimental data despite high R^2 concentration coefficient values and relatively small SSE values.

Temkin's model was not a good fit because the rising temperature was not beneficial for the adsorption system since this model describes an energy state where the heat of adsorption falls linearly down with an increased adsorption capacity.

The favourability of the Redlich–Peterson model to best describe the experimental data correctly is supported by the statistical indices value of R^2 and SSE. Also, the values obtained for 'g' are less than 1. This confirms the better fitting of the Redlich–Peterson model for all the studied temperatures, hence, an occurrence of a homogeneous as well as heterogeneous predominated surface adsorption of CR dye onto TNR@PEI. The values of SSE were applied to verify the model's validity. The SSE was found to be the smallest for all the studied temperatures as compared to those of the other models [51].

A comparison of adsorption capacities of surface-modified agricultural adsorbents is presented in Table 4. The adsorption capacity of TNR@PEI compares well with the other reported adsorbents, and there is some competitive for TNR@PEI for removal of CR from solution.

3.2.6. Thermodynamic

Thermodynamic behavior was investigated to explore the mechanism involved in the adsorption process [41,42]. The variation of dye removal efficiency to temperature was examined by the thermodynamic parameters, such as enthalpy ($\Delta H°$), Gibbs free energy ($\Delta G°$), and entropy ($\Delta S°$) were calculated from Eqs. (11)–(13).

Table 3
Parameters of adsorption isotherm models for CR adsorption

Langmuir	K_L	$q_{e,exp}$ (mg/g)	$q_{e,theo}$ (mg/g)	R^2	SSE
20°C	0.0245 + 0.0042	197 ± 7	193 ± 6	0.980	811
30°C	0.227 ± 0.069	274 ± 1	250 ± 9	0.957	3,870
40°C	0.0234 ± 0.0074	240 ± 1	227 ± 13	0.942	3,380
Freundlich	K_F	$1/n$		R^2	SSE
20°C	28.9 ± 4.8	0.296 ± 0.028		0.963	1,574
30°C	94.8 ± 9.5	0.166 ± 0.018		0.975	2,245
40°C	37.9 ± 2.3	0.278 ± 0.010		0.994	302
Koble–Corrigan	A_K	B_K	N	R^2	SSE
20°C	13.8 ± 1.7	0.0582 ± 0.0058	0.649 ± 0.034	0.997	103
30°C	98.0 ± 13.2	0.300 ± 0.046	0.416 ± 0.079	0.989	919
40°C	33.6 ± 1.8	0.0614 ± 0.0077	0.377 ± 0.022	0.998	71.2
Redlich–Peterson	K_{RP}	a_{RP}	g	R^2	SSE
20°C	9.90 ± 0.64	0.137 ± 0.015	0.847 ± 0.008	0.999	22.6
30°C	152 ± 52	1.16 ± 0.491	0.889 ± 0.019	0.990	818
40°C	129 ± 38	2.93 ± 0.94	0.746 ± 0.008	0.999	74.6
Temkin	A_T	B_T		R^2	SSE
20°C	−7.96 ± 4.86	30.0 ± 1.0		0.989	472
30°C	75.7 ± 7.4	30.1 ± 1.5		0.990	878
40°C	35.2 ± 9.7	26.9 ± 2.0		0.946	3,170

Table 4
Comparison of adsorption capacities of surface-modified agricultural adsorbents

Adsorbent	Modifying agent	q_m (mg/g)	Isotherm	Kinetic	References
TNR	Polyethylenimine	274	Redlich–Peterson	Pseudo-second-order	This work
Wheat straw	Polyethylenimine	89.7	Langmuir	Intraparticle diffusion	[7]
Pine cone powder	HCl solution	40.19	Freundlich	Pseudo-second-order	[10]
	Ethylenediamine	491.1	Langmuir	Pseudo-second-order	
Sugarcane bagasse	Diethylenetriamine	734.3	Langmuir	Pseudo-second-order	
	Triethylenetetramine	766	Langmuir	Pseudo-second-order	[17]
	Tetraethylenepentamine	790.7	Langmuir	Pseudo-second-order	
Chitosan	Beta-cyclodextrin zinc oxide composite	147.28	Langmuir	Pseudo-second-order	[24]
Wheat straw	Ethylenediamine	68.6	Langmuir	Pseudo-second-order	[32]
Starch	AlOOH–FeS$_2$	333.3	Freundlich	Pseudo-first-order	[42]
Wheat straw	Cetyltrimethyl ammonium bromide	71.2	Langmuir	Pseudo-first-order	[43]
Biomass of *Funalia trogii*	Iminodiacetic acid	153.6	Langmuir	Pseudo-second-order	[48]
Biomass of *Funalia trogii*	Triethylenetetramine	193.7	Langmuir	Pseudo-second-order	[48]
Guava leaf	H$_3$PO$_4$ activated carbon	47.62	Freundlich	Pseudo-second-order	[50]

$$\Delta G° = -RT \ln K_c \tag{11}$$

$$K_c = \frac{C_{ae}}{C_e} \tag{12}$$

$$\Delta G° = \Delta H° - T\Delta S° \tag{13}$$

$$\ln k_2 = -\frac{E_a}{RT} + \ln k_0 \tag{14}$$

where K_c is the distribution coefficient, R is the gas constant (8.314 J/mol K), T is the absolute temperature (K), C_{ae} and C_e are the equilibrium concentration of CR (mg/g) on the adsorbent, and in solution, k_2 is rate constant,

and E_a is activation energy; k_0 is a preexponential factor. The thermodynamic parameters obtained are listed in Table 5.

The negative values of $\Delta G°$ at all temperatures confirmed the feasibility and spontaneity of the adsorption process. Also, the absolute values of $\Delta G°$ (lower than 20 kJ/mol) suggest physisorption [41]. A positive value of $\Delta H°$ indicates the reaction was endothermic. The energy ($\Delta H°$) associated with physisorption are van der Waals forces (4–10 kJ/mol), hydrophobic interaction (5 kJ/mol), hydrogen bonding (2–40 kJ/mol), coordination exchange (40 kJ/mol), dipole bond forces (2–29 kJ/mol), and electrostatic interaction (20–80 kJ/mol). The adsorption process is primarily mediated by physisorption than a chemical since $\Delta H°$ is 20 kJ/mol [41]. The negative value for $\Delta S°$ confirmed the decreased randomness at the solid–solute interface during adsorption, which reflects the affinity of the TNR@PEI for CR and that the low value of $\Delta S°$ also reinforces no remarkable change in entropy. Besides, the quantity of activation energy, E_a obtained (0.751 kJ/mol) in this study fall within the range of 4–80 kJ/mol, confirming a physical adsorption process [43].

3.2.7. Regeneration performance

Regeneration performance is one of the most critical considerations in the applicability of adsorbents because of cost-effectiveness and concerns of secondary pollution [51–54]. In this study, the TNR@PEI after adsorption was eluted four times using 0.1 mol/L NaOH solutions in batch mode. This chosen elution solution was valid because the spent adsorbent had positive charges, and the NaOH solution could neutralize the positive charge of PEI chains on the TNR and reduce the electrostatic interaction between the CR and the TNR@PEI. Also, the OH⁻ from NaOH was competitive to bind these sites in a high alkaline condition. This leads to a weak interaction between the amino group on the adsorbent surface and the negative group ($-SO_3^-$) on the dye molecule. From the results obtained from this study, the efficiency of desorption was 73, 68, 62, and 60% with a concomitant regeneration efficiency of 93%, 86%, 84%, and 81% after four cycles, respectively.

A similar type of observation has been reported elsewhere; in the case of desorption of CR from PEI-grafted wheat straw [7], cetyl trimethyl ammonium bromide modified wheat straw [43], iminodiacetic acid and triethylenetetramine modified fungal biomass [47], CS/β-CD/nano-ZnO (CS – chitosan; CD – cyclodextrin) composite membrane [24], tamarind fruit shell [19] and Fe-doped CS-PVA (PVA – polyvinyl alcohol) film [19].

3.3. Proposed adsorption mechanism for CR by TNR@PEI

Adsorbents structure, functional behavior of the adsorbate molecule, surface characteristics of the adsorbent, mass

transport process are among the factors that influence the adsorption capacity of adsorbents [55,56]. From the analysis of results and discussions above, the electrostatic attraction might primarily mediate the adsorption process. Thus, in acidic conditions, the amino groups on the surface of TNR@PEI were protonated to form the ammonium ($-NH_3^+$) whiles the anionic group of CR ($-SO_3^-$) was available in solution, hence the positive-negative charge attraction (electrostatic forces) and hydrogen bonding. Moreover, CR being a planar molecule can readily be adsorbed on the cellulose-based adsorbents by hydrogen bonding interactions and van der Waals forces. Furthermore, the CR molecule contains a free amino end-group on the benzene ring; hence, hydrogen bonding might exit between TNR@PEI and CR. The FTIR spectra of the PEI modified cellulose-based adsorbent (TNR@PEI), and the dye loaded adsorbent (TNR@PEI@CR) showed the possible interaction sites between the modified adsorbents and CR dye molecules, thus, the sulfonyl from the CR and the ammonium ions and the OH from the adsorbent (Fig. 10). Compared with the spectra of TNR@PEI, the intensities of the characteristic peaks for the dye loaded adsorbent shrank and shifted slightly (Figs. 2 and 4). These indicated the specific electrostatic and hydrogen-bonding interactions between the functional groups of dye molecules and the TNR@PEI adsorbents. Fig. 10 depicts the proposed adsorption mechanism.

4. Conclusion

In this study, TNR@PEI with high amino density was prepared successfully by loading PEI onto the surface of TNR. A batch adsorption experiment corroborated that CR adsorption was highly depended on solution pH and was affected by ionic strength, which suggested that the adsorption was mainly attributed to ionic forces between the charged NH_3^+ and the anionic CR under acidic conditions. Besides, factors such as hydrogen bond or Van der Waals' force may be present in addition to the electrostatic attraction between the adsorbent. The batch experimental data were best described by the pseudo-second-order kinetic model and, the Redlich–Peterson model. These thermodynamic parameters underpinned an endothermic, spontaneous adsorption process. These results intimate physisorption coupled with ionic interaction mediated the adsorption of Congo red by TNR@PEI. Considering the results obtained herein, surface modified TNR can be used as a potential green eco-friendly agricultural waste material in the treatment of anionic dyes.

Table 5
Thermodynamic parameters of CR adsorption onto TNR@PEI

E_a (kJ/mol)	$\Delta H°$ (kJ/mol)	$\Delta S°$ (kJ/mol K)	$\Delta G°$ (kJ/mol)		
			293 K	303 K	313 K
0.751	20.0	−0.080	−1.46	−8.26	−3.06
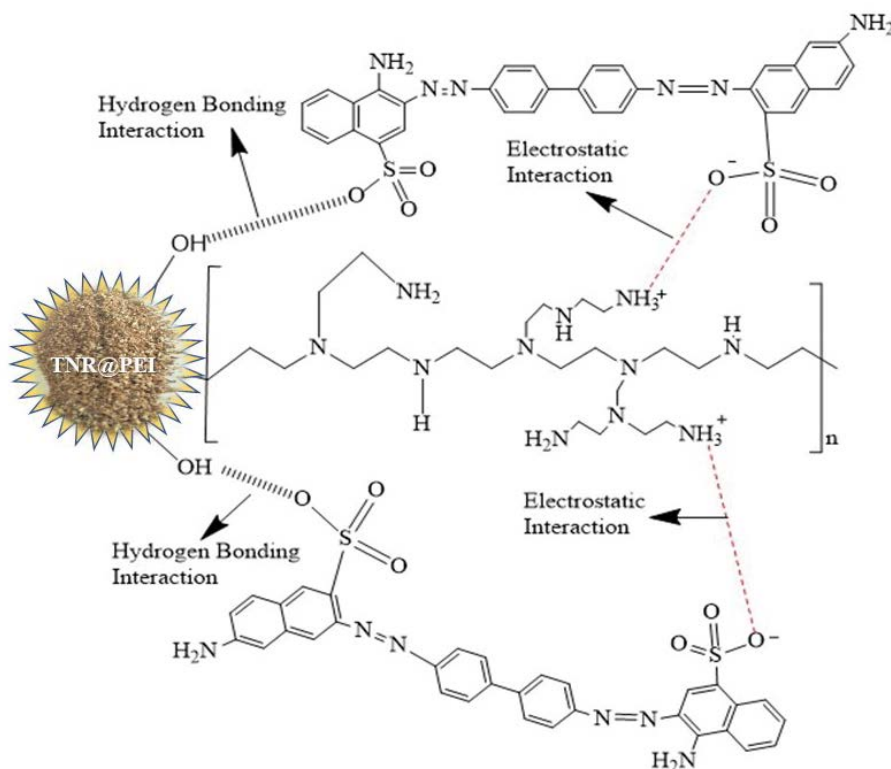
Fig. 10. Schematic drawing depicting the predicted interactions between the TNR@PEI and CR molecule.

References

[1] Y.B. Zhou, J. Lu, Y. Zhou, Y.D. Liu, Recent advances for dyes removal using novel adsorbents: a review, Environ. Pollut., 252 (2019) 352–365.

[2] S. Zwane, M.L. Masheane, A.T. Kuvarega, G.D. Vilakati, B.B. Mamba, H. Nyoni, S.D. Mhlanga, D.S. Dlamini, Polyethersulfone/*Chromolaena odorata* (PES/CO) adsorptive membranes for removal of Congo red from water, J. Water Process Eng., 30 (2019) 100498, https://doi.org/10.1016/j.jwpe.2017.09.013.

[3] C.M. da Silva Burigato Costa, L. da Silva Marques, A.K. Almeida, I.R. Leite, I.K. de Almeida, Applicability of water quality models around the world—a review, Environ. Sci. Pollut. Res., 26 (2019) 36141–36162.

[4] R.P. Han, D.D. Ding, Y.F. Xu, W.H. Zou, Y.F. Wang, Y.F. Li, L.N. Zou, Use of rice husk for the adsorption of Congo red from aqueous solution in column mode, Bioresour. Technol., 99 (2008) 2938–2946.

[5] F. Gimbert, N. Morin-Crini, F. Renault, P.-M. Badot, G. Crini, Adsorption isotherm models for dye removal by cationized starch-based material in a single component system: error analysis, J. Hazard. Mater., 157 (2008) 34–46.

[6] S.S. Chen, K. Wen, X.T. Zhang, R.Z. Zhang, R.P. Han, Adsorption of neutral red onto MIL-100(Fe) from solution: characterization, equilibrium, kinetics, thermodynamics and process design, Desal. Water Treat., 177 (2020) 197–208.

[7] Y. Shang, J.H. Zhang, X. Wang, R.D. Zhang, W. Xiao, S.S. Zhang, R.P. Han, Use of polyethylenimine-modified wheat straw for adsorption of Congo red from solution in batch mode, Desal. Water Treat., 57 (2016) 8872–8883.

[8] C.X. Zhu, Y.X. Xia, Y.Y. Zai, Y.Q. Dai, X.Y. Liu, J. Bian, Y. Liu, J.S. Liu, J.S. Liu, G.Y. Li, Adsorption and desorption behaviors of HPEI and thermoresponsive HPEI based gels on anionic and cationic dyes, Chem. Eng. J., 369 (2019) 863–873.

[9] K. Grace Pavithra, P. Senthil Kumar, V. Jaikumar, P. Sundar Rajan, Removal of colorants from wastewater: a review on sources and treatment strategies, J. Ind. Eng. Chem., 75 (2019) 1–19.

[10] S. Dawood, T.K. Sen, Removal of anionic dye Congo red from aqueous solution by raw pine and acid-treated pine cone powder as adsorbent: equilibrium, thermodynamic, kinetics, mechanism and process design, Water Res., 46 (2012) 1933–1946.

[11] G. Crini, E. Lichtfouse, Advantages and disadvantages of techniques used for wastewater treatment, Environ. Chem. Lett., 17 (2018) 145–155.

[12] M.N. Khan, O. Bashir, T.A. Khan, S.A. AL-Thabaiti, Z. Khan, CTAB capped synthesis of bio-conjugated silver nanoparticles and their enhanced catalytic activities, J. Mol. Liq., 258 (2018) 133–141.

[13] O. Bashir, M.N. Khan, T.A. Khan, Z. Khan, S.A. AL-Thabaiti, Influence of stabilizing agents on the microstructure of co-nanoparticles for removal of Congo red, Environ. Technol. Innovation, 8 (2017) 327–342.

[14] F.M. Mpatani, A.A. Aryee, A.N. Kani, Q.H. Guo, E. Dovi, L.B. Qu, Z.H. Li, R.P. Han, Uptake of micropollutant-bisphenol A, methylene blue and neutral red onto a novel bagasse-β-cyclodextrin polymer by adsorption process, Chemosphere, 259 (2020) 127439, https://doi.org/10.1016/j.chemosphere.2020.127439.

[15] A.A. Aryee, F.M. Mpatani, A.N. Kani, E. Dovi, R.P. Han, Z.H. Li, L.B. Qu, Iminodiacetic acid functionalized magnetic peanut husk for the removal of methylene blue from solution: characterization and equilibrium studies, Environ. Sci. Pollut. Res., 27 (2020) 40316–40330.

[16] C. Liao, X.-R. Zhao, X.-Y. Jiang, J. Teng, J.-G. Yu, Hydrothermal fabrication of novel three-dimensional graphene

oxide-pentaerythritol composites with abundant oxygen-containing groups as efficient adsorbents, Microchem. J., 152 (2020) 104288, https://doi.org/10.1016/j.microc.2019.104288.

[17] A.T. Ojedokun, O.S. Bello, Kinetic modeling of liquid-phase adsorption of Congo red dye using guava leaf-based activated carbon, Appl. Water Sci., 7 (2017) 1965–1977.

[18] R. Ahmad, R. Kumar, Adsorptive removal of Congo red dye from aqueous solution using bael shell carbon, Appl. Surf. Sci., 257 (2010) 1628–1633.

[19] K. Wen, Y. Li, S.X. Zhang, X.T. Zhang, R.P. Han, Adsorption of Congo red from solution by iron doped PVA-chitosan composite film, Desal. Water Treat., 187 (2020) 378–389.

[20] M.M. Yang, X.Y. Li, W.L. Wang, S.S. Zhang, R.P. Han, Adsorption of methyl blue from solution by carboxylic multi-walled carbon nanotubes in batch mode, Desal. Water Treat., 159 (2019) 365–376.

[21] Y.F. Gu, M.M. Yang, W.L. Wang, R.P. Han, Phosphate adsorption from solution by zirconium-loaded carbon nanotubes in batch mode, J. Chem. Eng. Data, 64 (2019) 2849–2858.

[22] C.D. Qi, H.Z. Chen, C.M. Xu, Z. Xu, H.B. Chen, S.G. Yang, S.Y. Li, H. He, C. Sun, Synthesis and application of magnetic materials-barium ferrite nanomaterial as an effective microwave catalyst for degradation of brilliant green, Chemosphere, 260 (2020) 127681, https://doi.org/10.1016/j.chemosphere.2020.127681.

[23] H.X. Lyu, K. Hu, J.S. Fan, Y.X.F. Ling, Z.H. Xie, J.X. Li, 3D hierarchical layered double hydroxide/carbon spheres composite with hollow structure for high adsorption of dye, Appl. Surf. Sci., 500 (2020) 144037, https://doi.org/10.1016/j.apsusc.2019.144037.

[24] X.C. Yan, X.P. Zhang, Q. Li, Preparation and characterization of CS/β-CD/Nano-ZnO composite porous membrane optimized by Box-Behnken for the adsorption of Congo red, Environ. Sci. Pollut. Res., 25 (2018) 22244–22258.

[25] Y. Ma, B.W. Zhang, H.J. Ma, M. Yu, L.F. Li, J.Y. Li, Polyethylenimine nanofibrous adsorbent for highly effective removal of anionic dyes from aqueous solution, Sci. China Mater., 59 (2016) 38–50.

[26] A.A. Aryee, F.M. Mpatani, X.T. Zhang, A.N. Kani, E. Dovi, R.P. Han, Z.H. Li, L.B. Qu, Iron(III) and iminodiacetic acid functionalized magnetic peanut husk for the removal of phosphate from solution: characterization, kinetic and equilibrium studies, J. Cleaner Prod., 268 (2020) 122191, https://doi.org/10.1016/j.jclepro.2020.122191.

[27] F.M. Mpatani, A.A. Aryee, A.N. Kani, K. Wen, E. Dovi, L.B. Qu, Z.H. li, R.P. Han, Removal of methylene blue from aqueous medium by citrate modified bagasse: kinetic, equilibrium and thermodynamic study, Bioresour. Technol. Rep., 11 (2020) 100463, https://doi.org/10.1016/j.biteb.2020.100463.

[28] A.N. Kani, E. Dovi, F.M. Mpatani, Z.H. Li, R.P. Han, L.B. Qu, Tiger nut residue as a renewable adsorbent for methylene blue removal from solution: adsorption kinetics, isotherm, and thermodynamic studies, Desal. Water Treat., 191 (2020) 426–437.

[29] M.R. Oliveira, M.M. Oliveira, R.J. Oliveira, A. Dervanoski, E. Franceschi, S.M. Egues, J.F. de Conto, Amine-modified silica surface applied as adsorbent in the phenol adsorption assisted by ultrasound, Chem. Eng. Commun., 206 (2019) 1554–1569.

[30] M. Kousha, E. Daneshvar, M.S. Sohrabi, M. Jokar, A. Bhatnagar, Adsorption of acid orange II dye by raw and chemically modified brown macroalga *Stoechospermum marginatum*, Chem. Eng. J., 192 (2012) 67–76.

[31] S.T. Ong, C.K. Lee, Z. Zainal, Removal of basic and reactive dyes using ethylenediamine modified rice hull, Bioresour. Technol., 98 (2007) 2792–2799.

[32] Z.W. Wang, P. Han, Y.B. Jiao, D. Ma, C.C. Dou, R.P. Han, Adsorption of Congo red using ethylenediamine modified wheat straw, Desal. Water Treat., 30 (2011) 195–206

[33] M.S. Sajab, C.H. Chia, S. Zakaria, P.S. Khiew, Cationic and anionic modifications of oil palm empty fruit bunch fibers for the removal of dyes from aqueous solutions, Bioresour. Technol., 128 (2013) 571–577.

[34] Y.H. Li, H.X. Zhu, C.Z. Zhang, M.X. Cheng, H. He, PEI-grafted magnetic cellulose for Cr(VI) removal from aqueous solution, Cellulose, 25 (2018) 4757–4769.

[35] J.L. Wang, C. Chen, Biosorbents for heavy metals removal and their future, Biotechnol. Adv., 27 (2009) 195–226.

[36] J.J. Dong, Y.Y. Du, R.S. Duyu, Y. Shang, S.S. Zhang, R.P. Han, Adsorption of copper ion from solution by polyethylenimine modified wheat straw, Bioresour. Technol. Rep., 6 (2019) 96–102.

[37] S.B. Deng, Y.-P. Ting, Characterization of PEI-modified biomass and biosorption of Cu(II), Pb(II) and Ni(II), Water Res., 39 (2005) 2167–2177.

[38] X. Xu, B.Y. Gao, B. Jin, Q.Y. Yue, Removal of anionic pollutants from liquids by biomass materials: a review, J. Mol. Liq., 215 (2016) 565–595.

[39] L. Meili, P.V.S. Lins, M.T. Costa, R.L. Almeida, A.K.S. Abud, J.I. Soletti, G.L. Dotto, E.H. Tanabe, L. Sellaoui, S.H.V. Carvalho, A. Erto, Adsorption of methylene blue on agro-industrial wastes: experimental investigation and phenomenological modelling, Prog. Biophys. Mol. Biol., 141 (2019) 60–71.

[40] S.B. Deng, Y.P. Ting, Polyethylenimine-modified fungal biomass as a high-capacity biosorbent for Cr(VI) anions: sorption capacity and uptake mechanisms, Environ. Sci. Technol., 39 (2005) 8490–8496.

[41] R. Kumar, J. Rashid, M.A. Barakat, Synthesis and characterization of a starch-AlOOH-FeS$_2$ nanocomposite for the adsorption of Congo red dye from aqueous solution, RSC Adv., 4 (2014) 38334–38340.

[42] S. Rongpipi, D. Ye, E.D. Gomez, E.W. Gomez, Progress and opportunities in the characterization of cellulose - an important regulator of cell wall growth and mechanics, Front. Plant Sci., 9 (2019) 1–28.

[43] R.D. Zhang, J.H. Zhang, X.N. Zhang, C.C. Dou, R.P. Han, Adsorption of Congo red from aqueous solutions using cationic surfactant modified wheat straw in batch mode: kinetic and equilibrium study, J. Taiwan Inst. Chem. Eng., 45 (2014) 2578–2583.

[44] M.C.S. Reddy, L. Sivaramakrishna, A.V. Reddy, The use of an agricultural waste material, Jujuba seeds for the removal of anionic dye (Congo red) from aqueous medium, J. Hazard. Mater., 203–204 (2012) 118–127.

[45] M.A.M. Salleh, D.K. Mahmoud, W.A.W.A. Karim, A. Idris, Cationic and anionic dye adsorption by agricultural solid wastes: a comprehensive review, Desalination, 280 (2011) 1–13.

[46] R. Kumar, R.Kr. Sharma, A.P. Singh, Removal of organic dyes and metal ions by cross-linked graft copolymers of cellulose obtained from the agricultural residue, J. Environ. Chem. Eng., 6 (2018) 6037–6048.

[47] G. Bayramoglu, M.Y. Arica, Adsorption of Congo red dye by native amine and carboxyl modified biomass of *Funalia trogii*: isotherms, kinetics and thermodynamics mechanisms, Korean J. Chem. Eng., 35 (2018) 1303–1311.

[48] J.-X. Yu, W.-L. Xiong, J. Zhu, J.-D. Chen, R.-A. Chi, Removal of Congo red from aqueous solution by adsorption onto different amine compounds modified sugarcane bagasse, Clean Technol. Environ. Policy, 19 (2017) 517–525.

[49] M. Butnariu, P. Negrea, L. Lupa, M. Ciopec, A. Negrea, M. Pentea, I. Sarac, I. Samfira, Remediation of rare earth element pollutants by sorption process using organic natural sorbents, Int. J. Environ. Res. Public Health, 12 (2015) 11278–11287.

[50] N. Belachew, G. Bekele, Synergy of magnetite intercalated bentonite for enhanced adsorption of Congo red dye, Silicon, 12 (2020) 603–612.

[51] A.J. Jadhav, V.C. Srivastava, Multicomponent adsorption isotherm modeling using thermodynamically inconsistent and consistent models, AIChE J., 65 (2019) e16727, https://doi.org/10.1002/aic.16727.

[52] T. Zhou, W.Z. Lu, L.F. Liu, H.M. Zhu, Y.B. Jiao, S.S. Zhang, R.P. Han, Effective adsorption of light green anionic dye from solution by CPB modified peanut in column mode, J. Mol. Liq., 211 (2015) 909–914.

[53] B.L. Zhao, W. Xiao, Y. Shang, H.M. Zhu, R.P. Han, Adsorption of light green anionic dye using cationic surfactant-modified

peanut husk in batch mode, Arabian J. Chem., 10 (2017) S3595–S3602.

[54] Y.Y. Hu, R.P. Han, Selective and efficient removal of anionic dyes from solution by zirconium(IV) hydroxide-coated magnetic materials, J. Chem. Eng. Data, 64 (2019) 791–799.

[55] M.C.S. Reddy, Removal of direct dye from aqueous solutions with an adsorbent made from tamarind fruit shell, an agricultural solid waste, J. Sci. Ind. Res. (India), 65 (2006) 443–446.

[56] M.Y. Liu, X.T. Zhang, Z.H. Li, L.B. Qu, R.P. Han, Fabrication of zirconium (IV)-loaded chitosan/Fe_3O_4/graphene oxide for efficient removal of alizarin red from aqueous solution, Carbohydr. Polym., 248 (2020) 116792, https://doi.org/10.1016/j.carbpol.2020.116792.